

LETTER TO THE EDITOR

Weakening of magnetic braking in cataclysmic variables explains the dearth of period bouncers

Arnab Sarkar¹, Antonio C. Rodriguez², Sivan Ginzburg³, Lev Yungelson⁴ and Christopher A. Tout¹

¹ Institute of Astronomy, The Observatories, Madingley Road, Cambridge CB3 0HA, UK
e-mail: as3158@cam.ac.uk

² Department of Astronomy, California Institute of Technology, Pasadena, CA 91125, USA

³ Racah Institute of Physics, The Hebrew University, Jerusalem 91904, Israel

⁴ Institute of Astronomy of the Russian Academy of Sciences, 48 Pyatnitskaya Str., 119017 Moscow, Russia

Received xx; accepted xx

ABSTRACT

Context. Period bouncers are cataclysmic variables (CVs) that have evolved past their orbital period minimum. The strong disagreement between theory and observations of the relative fraction of period bouncers is a severe shortcoming in the understanding of CV evolution.

Aims. We test the implications of the hypothesis that magnetic braking (MB), which is suggested to be an additional angular momentum loss (AML) mechanism for CVs below the period gap ($P_{\text{orb}} \lesssim 120$ min), weakens around their period minimum.

Methods. We compute the evolution of CV donors below the period gap using the MESA code, assuming that the evolution of the system is driven by AML by gravitational wave radiation (GWR) and MB. We parametrize the MB strength as $\text{AML}_{\text{MB}} = \kappa \text{AML}_{\text{GWR}}$.

We compute two qualitatively different sets of models, one where κ is a constant and the other where κ depends on stellar parameters.

Results. We find that in the latter set of models, κ decreases as the CV approaches the period minimum ($P_{\text{orb}} \approx 80$ min), beyond which $\kappa \approx 0$. This stalls their evolution so that they spend a long time in the observed period minimum spike ($80 \lesssim P_{\text{orb}}/\text{min} \lesssim 86$). Here they become difficult to distinguish from pre-bounce systems in the spike. A strong decrease in mass-transfer rate makes them virtually undetectable as they evolve further. We also discuss the physical processes, such as dynamo action, white dwarf magnetism and dead zones, that may cause such a weakening of MB at short orbital periods.

Conclusions. The weakening magnetic braking formalism solves the problem of the lack of period bouncers in CV observational surveys.

Key words. binaries: close – stars: magnetic field — novae, cataclysmic variables — white dwarfs – stars: late-type – brown dwarfs

1. Introduction

One of the most important challenges in our understanding of the evolution of cataclysmic variables (CVs, Warner 2003) is period bouncers. These are CVs that, according to the theory of CV evolution, widen their orbital separation after reaching a minimum in their orbital period P_{orb} owing to an interplay between their mass-loss timescale, thermal timescale and degeneracy (Paczynski & Sienkiewicz 1981). However, the predicted fraction of period bouncers (70% by Kolb 1993, 40% by Goliaš & Nelson 2015) is much greater than that inferred observationally (14% by Pala et al. 2020). Recent surveys have further exacerbated this disagreement with the claim that the fraction of period bouncers in CV population does not exceed more than a few percent (Inight et al. 2023).

It was pointed out by Pala et al. (2020) that it is possible that the current models of CV evolution (e.g. Knigge et al. 2011) do not correctly describe their evolution. An important ingredient governing the evolution of such CVs is magnetic braking (MB). It is well established now that there may be a mechanism of angular momentum loss (AML) operating below the period gap (P_{gap} , $2 \lesssim P_{\text{orb}}/\text{hr} \lesssim 3$) in addition to AML by gravitational wave radiation (GWR). This is because the period minimum $P_{\text{min}} \approx 65$ min by a system evolved solely with AML_{GWR} . This disagrees with observations, which find $P_{\text{min}} \approx 80$ min

(Gänsicke et al. 2009). Knigge et al. (2011) reported that a MB strength $\text{AML}_{\text{MB}} = 1.47 \text{AML}_{\text{GWR}}$ below the period gap can reproduce P_{min} correctly for CV tracks. Solely based on this result, several works have used this constant multiplicative factor to model CV donors at short P_{orb} . However, very little progress has been made in understanding the physics of MB (Sarkar et al. 2023) and there is no evidence that AML_{MB} in short-period CVs can be simply described by a scaling factor applied to AML_{GWR} . In addition, it is unlikely that this scaling factor remains constant throughout the evolution of these CVs.

Here we study the implications of a MB mechanism the strength of which weakens as the CV evolves towards P_{min} to explain the dearth of observed period bouncers. In Sect. 2 we describe our weakening MB paradigm and illustrate its results. In Sect. 3 we discuss the physical processes that can weaken MB in short-period CVs. We conclude in Sect. 4.

2. The weakening magnetic braking paradigm

Here we describe our approach to study the implications of a MB strength that weakens around the CV period minimum.

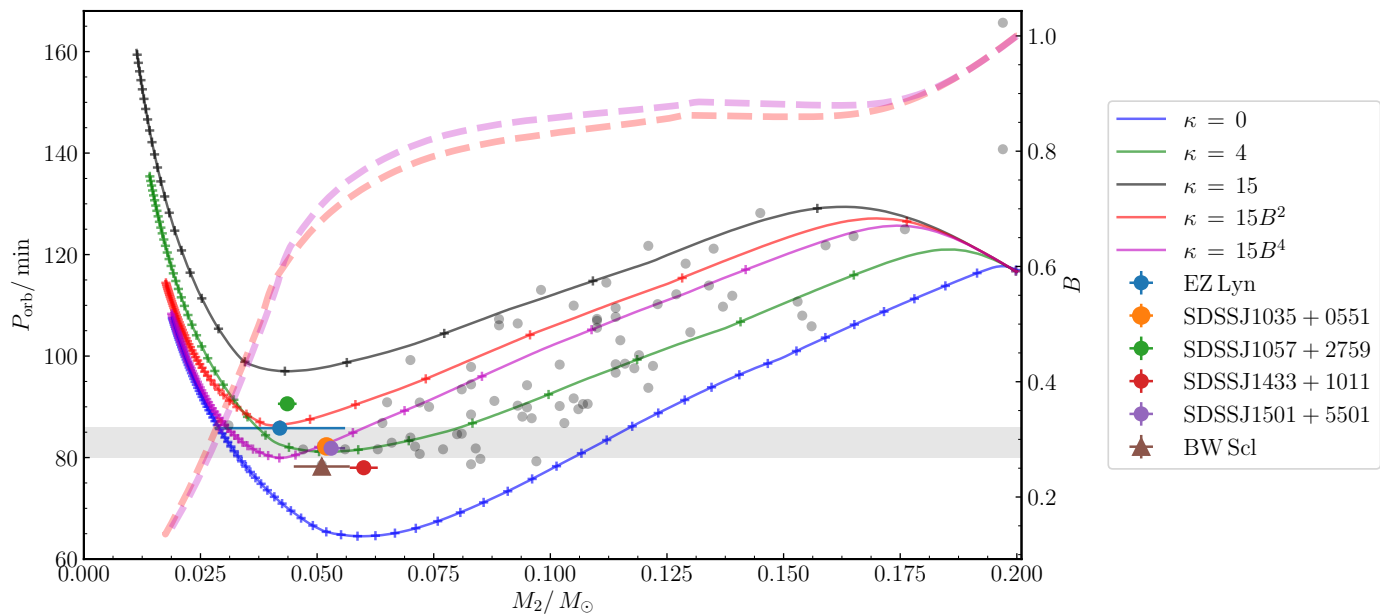


Fig. 1. The evolution of CVs below the period gap. The solid lines show the tracks in the $M_2 - P_{\text{orb}}$ plane (lower x- and left y-axis). The dashed tracks in the $M_2 - B$ plane (lower x- and right y-axis) show the evolution of B (Eq. (1)) for the models where κ depends on stellar parameters. The pluses on each solid track denote timesteps of 100 Myr. The different colors correspond to different κ s. The grey points are CVs reported by Knigge (2006, their Table 1). We also plot observed period bouncer candidates from Table A.1. Eclipsing systems are plotted as circles while non-eclipsing systems are plotted as triangles. The horizontal shaded region is the observed period minimum spike ($80 \lesssim P_{\text{orb}}/\text{min} \lesssim 86$) reported by Gänsicke et al. (2009).

2.1. Binary evolution calculation

We compute the evolution of CVs starting from a detached system with a fully convective donor of mass $M_{2,i} = 0.2M_{\odot}$, a WD accretor of mass $M_{1,i} = M_{\text{WD},i} = 0.8M_{\odot}$ and an initial period $P_{\text{orb},i} = 3.18\text{ hr}$ using version r23.05.1 of MESA (Paxton et al. 2011, 2013, 2015, 2018, 2019; Jermyn et al. 2023). The system parameters are chosen such that $P_{\text{orb},i}$ is the upper limit of P_{gap} and $M_{2,i}$ is the donor mass at P_{gap} as reported by Knigge et al. (2011). All the results we obtain are by modifying `jdot_multiplier` in `project_inlist` in the MESA code which multiplies AML_{GWR} by the factor `jdot_multiplier`. We call this factor $1 + \kappa$. We define κ as a parametrized estimate of the strength of AML_{MB} . This approach is similar to that of Knigge et al. (2011). However, here κ may also depend on stellar parameters (Sect. 2.2). We assume fully conservative mass transfer so that the only mechanisms of AML are GWR and MB.

We note importantly that no unique $M_{2,\text{gap}}$ exists for all CVs, as known from observations and theoretical computations (e.g. Knigge et al. 2011 and Sarkar & Tout 2022). This is because $M_{2,\text{gap}}$ and the lower end of the period gap, where mass transfer resumes ($P_{\text{gap,-}}$), depend on M_1 and the MB strength above the period gap. If we assume that the initial strength of MB below the period gap depends on stellar parameters, $M_{2,\text{gap}}$ and $P_{\text{gap,-}}$ set the initial κ of our systems. In the next section, we choose how κ behaves as the CV evolves.

2.2. The method

Consider two qualitatively different sets of models. One where κ is a constant throughout, and the other where κ varies with stellar parameters. In the first set, we compute models evolved with $\kappa = 0, 4$ and 15 (Fig. 1). The latter two κ s are purely ad hoc and have been chosen to aid the understanding of a MB that depends on stellar parameters, described later. The system with

$\kappa = 0$ evolves solely with GWR and represents the minimum P_{orb} for a given M_2 . Systems such as polars (AM Her systems, Li et al. 1994), where there is no MB, follow this track. In unevolved CVs with some degree of MB, $\kappa > 0$ initially. We plot in Fig. 1 CVs with donor masses and periods, estimated from superhump periods¹ assuming $M_1 = 0.75M_{\odot}$ by Knigge (2006, their Table 1)². There is quite a bit of scatter among these points and they do not seem to converge on a unique evolutionary track. This illustrates that varying strengths of MB likely operate below the period gap³. However, studying the significance of this effect is beyond the scope of this letter. The track with $\kappa = 15$ matches with the systems with the biggest P_{orb} for a given M_2 in the catalog of Knigge (2006). So, hereinafter, we assume that the tracks with $\kappa = 15$ and $\kappa = 0$ exhibit respectively the upper and lower limits of P_{orb} for a given M_2 .

Consider the other set of tracks where κ varies with stellar parameters. This set illustrates the behavior of the system when the strength of MB depends on stellar structure and changes as the donor evolves. We use the result of the strong- and weak-field dynamo for fully convective low-mass stars proposed by Morin et al. (2011) to model such a MB strength. They argue, based on spectropolarimetric observations by Morin et al. (2010), that two different magnetic field profiles exist in isolated fully convective stars with similar rotation rates and masses. The first is a strong and steady axial dipole field and the second is a weak multipolar non-axisymmetric field that is changing rapidly. Be-

¹ We do not see any CVs in the catalog of Knigge (2006) following the zero MB track in Fig. 1. This is because superhumps are a result of donor-induced eccentricity in their accretion disk and polars do not form an accretion disk.

² These are pre-bounce CVs. The M_2 for post-bounce CVs is calculated differently (Sect. 2.3).

³ We note that the scatter of the systems in the catalog of Knigge (2006) may be the result of other processes, such as irradiation of the donor by the WD, which can alter the thermal timescale of the donor.

cause donors in short-period CVs are fully convective, it is possible that a strong-field dynamo also operates in such CV donors where it drives MB. So, we use the formula for the magnetic field given by Morin et al. (2011, their Eq. (2)) to define κ . For details on how they derive their magnetic field expression, we urge the reader to refer to their Sect. 4.2. Other physical mechanisms that may lead to a stellar-dependent κ are discussed in Sect. 3.

We define a dimensionless quantity B as a proxy for the magnetic field as⁴

$$B = \frac{6 \text{ kG}}{19.5 \text{ kG}} \left(\frac{M_2}{M_\odot} \right)^{1/2} \left(\frac{R_2}{R_\odot} \right)^{-1} \left(\frac{L_2}{L_\odot} \right)^{1/6} \left(\frac{P_{\text{orb}}}{\text{d}} \right)^{-1/2}, \quad (1)$$

where R_2 and L_2 are the radius and the luminosity of the donor. We compute these using MESA. The last term in Eq. (2) of Morin et al. (2011) is $(P_{\text{spin}}/\text{d})^{-1/2}$, where P_{spin} is the spin period of the M-dwarf. This becomes $(P_{\text{orb}}/\text{d})^{-1/2}$ in our Eq. (1) because of tidal locking. The denominator 19.5 kG is the dipolar field at the time of the commencement of Roche lobe overflow (RLOF). This ensures that $B < 1$ throughout the evolution. We plot two tracks where $\kappa = 15 B^2$ and $\kappa = 15 B^4$. The exponents are ad hoc but highlight the varying degrees of the dependence of MB strength on the magnetic field, and hence, the stellar structure. They also lead to the system attaining P_{min} at 86 and 80 min respectively (Fig. 1), which are the upper and lower limit of the observed period minimum spike reported by Gänsicke et al. (2009). The behavior of B can be understood as follows. Because of RLOF and the fact that the donors are close to thermal equilibrium, R_2 , L_2 and P_{orb} are functions of M_2 , and so $B \equiv B(M_2)$. $P_{\text{orb}} \propto R_2^{3/2} M_2^{-1/2}$. For our donors $L_2 \propto M_2^\beta$, where $2 \lesssim \beta \lesssim 4$. If we define $R_2 \propto M_2^\alpha$, we get $B \propto M_2^{3/4+\beta/6-7\alpha/4}$. We have $\alpha > 0$ pre-bounce and $\alpha \lesssim 0$ post-bounce. Choosing $\beta = 3$, $\alpha = 0.6$ pre-bounce and $\alpha = 0.3$ post-bounce (similar to eq. (16) of Knigge et al. 2011), we get $B \propto M_2^{0.2}$ pre-bounce and $B \propto M_2^{0.725}$ post-bounce. So, post-bounce B decreases strongly because of a change in the $M_2 - R_2$ relation of the donor. The evolution of B is shown in Fig. 1.

2.3. Results

We follow the evolution of the models with $\kappa = 15 B^2$ and $\kappa = 15 B^4$ in the $M_2 - P_{\text{orb}}$ plane. At $M_2 \approx 0.2 M_\odot$, these systems are driven by strong MB so they follow the track with $\kappa = 15$. However, B starts decreasing gradually at $M_2 \approx 0.125 M_\odot$ and substantially when $M_2 \lesssim 0.05 M_\odot$. This leads to the weakening of the MB strength in these systems. We note importantly that for all our models, the absolute value of AML decreases as the CV evolves (see Appendix B). So, when we say ‘weakening’ of MB, we mean the additional weakening of the MB strength caused by B (Fig. B.1). The weakening of MB is such that the donor star always adjusts to it on its thermal timescale. The extent of the weakening depends on the power of B . Close to their respective P_{min} , MB becomes negligible. This can be understood with Eq. (1)–further evolution decreases M_2 and increases R_2 and, as a consequence, P_{orb} . These systems, now only driven by GWR, evolve further to join the $\kappa = 0$ track. This causes their evolution timescale to drastically increase around and beyond their P_{min} . Owing to their long evolutionary timescales, these systems stall

⁴ There is an additional term $(\eta_\odot/\eta_{\text{ref}})^{1/2}$ in the expression of the magnetic field in Morin et al. (2011). Here $\eta_{\text{ref}} \equiv 10^{11} \text{ cm}^2 \text{ s}^{-1}$ is the magnetic diffusivity and η_\odot is the reference magnetic diffusivity. Studying how this term varies for our CVs is beyond the scope of this work. So we set $(\eta_\odot/\eta_{\text{ref}}) = 1$.

in the period minimum spike and spend a lot of time there compared to systems evolved with a constant κ . This can be seen with the pluses marked on each track in Fig. 1 that denote a time interval of 100 Myr. Around their period minimum, the pluses are concentrated much more in the $\kappa = 15 B^4$ track than in the $\kappa = 4$ track. We define period bouncer CVs as systems with a brown dwarf donor ($M_2 \leq 0.07 M_\odot$) with $P_{\text{orb}} \geq 80$ min (Pala et al. 2020) and calculate the amount of time each of our models spends in the period minimum spike as a period bouncer. Although the tracks with $\kappa = 4$ and $\kappa = 15 B^4$ have approximately the same P_{min} , the latter spends about 1.2 Gyr as a bouncer, while the former spends only about 0.44 Gyr. Because the systems are clustered around the period minimum spike, it is very difficult to distinguish between pre-bounce and post-bounce systems observationally (Pala et al. 2018). We highlight that the weakening MB models also reproduce the period minimum reported by Knigge et al. (2011) but that the M_2 at which P_{min} is attained is much smaller than the $0.069 M_\odot$ reported by Knigge et al. (2011). So, if MB weakens in near- P_{min} CVs, our models suggest that most of the period bouncer candidates in Fig. 1 are pre-bounce CVs.

We also analyse our models in the $\dot{M}_2 - P_{\text{orb}}$ plane in Fig. 2. We compute the accretion rate of a system \dot{M}_2 using the relation derived by Townsley & Bildsten (2004),

$$L_{\text{WD}} = 10^{-3} L_\odot \left(\frac{\dot{M}_2}{10^{-10} M_\odot \text{ yr}^{-1}} \right) \left(\frac{M_{\text{WD}}}{0.9 M_\odot} \right)^{0.4} \quad (2)$$

which relates the WD mass, radius, and temperature to the accretion rate (Table A.1). It is also possible to estimate accretion rates from the X-ray luminosity or disk luminosity. The former requires a model of the X-ray emission mechanism, and the latter a model of disk geometry. Both require an estimate of accretion efficiency, which is often parameterized as η in the following:

$$L = \frac{\eta}{2} \frac{GM_{\text{WD}} \dot{M}_2}{R_{\text{WD}}} \quad (3)$$

where R_{WD} is the WD radius and L is the observed accretion luminosity (either from the disk or from the boundary layer, in X-rays). However, the range of η in CVs is a subject of current debate (see Sect. 6.1 of Mukai 2017 for a thorough explanation). As an example, one model of accretion is advective dominated accretion flow (ADAF), which was first applied to explain the hard X-ray spectra of CVs in Narayan & Popham (1993). It was later extended in Narayan et al. (1996) to X-ray binaries observed in a low accretion state. In this work, accretion efficiencies were shown to be very low, with η between 10^{-3} to 10^{-4} . From Eq. (3), it is clear how failing to incorporate low efficiencies could lead to an underestimate of accretion rate, given an observed luminosity. More recently, Liu et al. (2008) applied the ADAF model to X-ray spectra of CVs and found good agreement. Nevertheless, Mukai (2017) warns that a complete analysis of accretion efficiency in CVs, which takes into account interactions between disk annuli, is still needed. Later we demonstrate the sensitivity of our predictions to the method of obtaining \dot{M}_2 .

All our candidate bouncer CVs (Table A.1) with mass transfer via RLOF⁵ have \dot{M}_2 (estimated by Eq. (2)) about a few times $10^{-11} M_\odot \text{ yr}^{-1}$ (also see Pala et al. 2022, where all $\dot{M}_2 >$

⁵ Three magnetic CVs have been discovered with $\dot{M}_2 \approx 10^{-14} M_\odot \text{ yr}^{-1}$ (Muñoz-Giraldo et al. 2023). These mass-transfer rates are two orders of magnitude smaller than that predicted by the model evolved with GR. This may be because the mass-transfer rates are underestimated (see the discussion on Eq. 3).

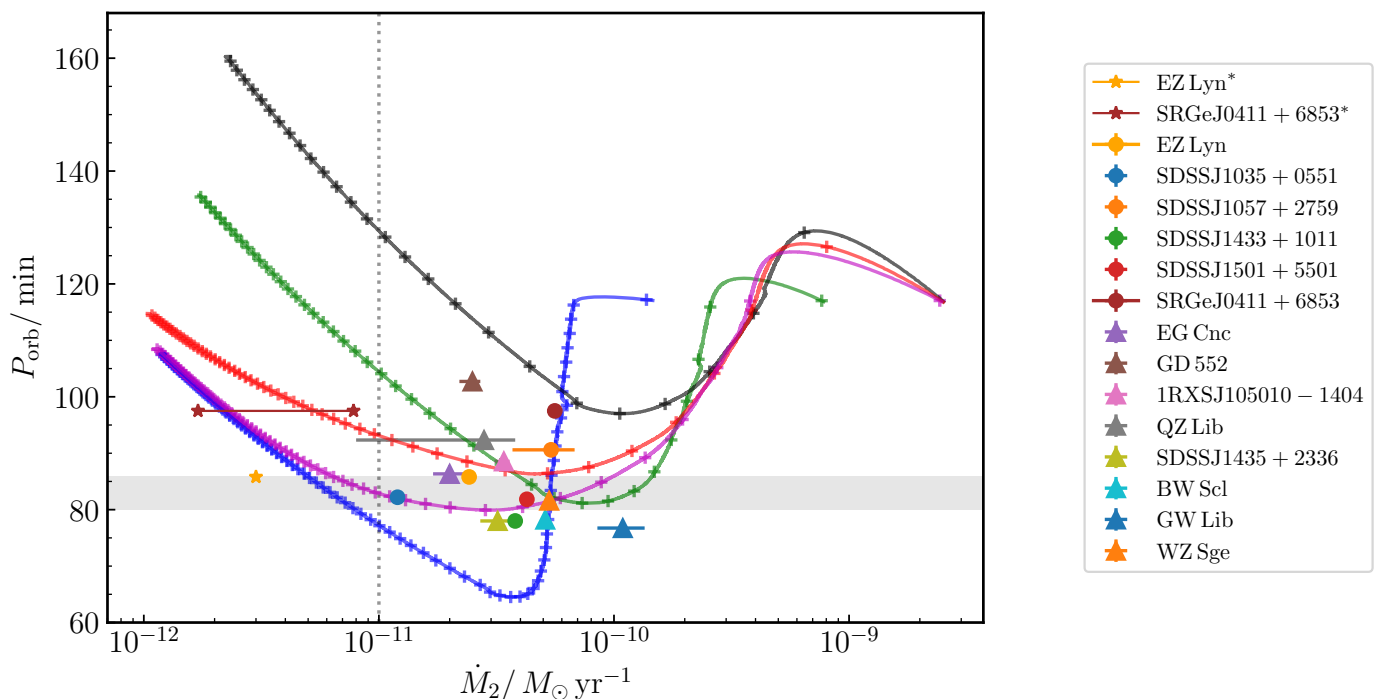


Fig. 2. The evolution of CVs below the period gap. Solid lines show evolution in the $P_{\text{orb}} - \dot{M}_2$ plane for the same tracks as in Fig. 1. Pluses on each track denote timesteps of 100 Myr. The dotted vertical line denotes $\dot{M}_2 = 10^{-11} M_{\odot} \text{yr}^{-1}$. Observed period bouncer candidates from Table A.1 are also plotted. Eclipsing systems are plotted as circles while non-eclipsing systems are plotted as triangles. The systems labeled and marked with stars have their \dot{M}_2 derived from X-ray luminosity (see the discussion in Sect. 2.3). The horizontal shaded region is the observed period minimum spike ($80 \leq P_{\text{orb}}/\text{min} \leq 86$) reported by Gänsicke et al. (2009).

$10^{-11} M_{\odot} \text{yr}^{-1}$). So we assume an optimistic detection threshold of $\dot{M}_2 = 10^{-11} M_{\odot} \text{yr}^{-1}$ such that any system below this limit is undetectable. This is likely to change with emerging data from optical and X-ray surveys, such as SDSS-V (Kollmeier et al. 2017) and SRG/eROSITA (Predehl et al. 2021; Sunyaev et al. 2021), respectively. The former has already led to the discovery of new period bouncer candidates, optically fainter than much of the population (Inight et al. 2023). The latter is 5 to 15 times deeper than the last all-sky X-ray survey, potentially revealing systems with lower accretion rates, for instance, the bouncer candidate reported by Galiullin et al. (2024). In addition, Rodriguez (2024) has presented a method to discover optically faint CVs such as period minimum and period bouncer systems using their X-ray/optical properties. This could reveal new systems in upcoming SRG/eROSITA data.

Under the above assumption on detection, the system with $\kappa = 15B^4$ never emerges from the period minimum spike as a detectable period bouncer. This track explains observed candidates clustered at the lower end of the period minimum spike in Fig. 2. The track with $\kappa = 15B^2$ bounces at about 86 min but becomes undetectable at about 90 min. This track explains observed candidates clustered at the upper end of the period minimum spike. The system with $\kappa = 4$ emerges from the period minimum spike with $\dot{M}_2 > 10^{-11} M_{\odot} \text{yr}^{-1}$. So, if such a constant κ is at play post bounce, there should be systems populating the region with $86 \leq P_{\text{orb}}/\text{min} \leq 105$ and $\dot{M}_2 \gtrsim 10^{-11} M_{\odot} \text{yr}^{-1}$. These are not observed, indicating further that MB weakens post-period minimum. Once SRG/eROSITA unveils systems with $\dot{M}_2 \approx 10^{-12} M_{\odot} \text{yr}^{-1}$, the $\kappa = 15B^4$ track indicates a population of systems upto $P_{\text{orb}} \approx 110$ min and the $\kappa = 15B^2$ track upto $P_{\text{orb}} \approx 115$ min.

It is important to note that our accretion rate estimates, based on WD properties (Eq. (2)), place the accretion rates of systems such as EZ Lyn (Amantayeva et al. 2021) and SRGeJ0411+6853 (Galiullin et al. 2024) nearly an order of magnitude higher than that reported by authors using X-ray or disk luminosities. Amantayeva et al. (2021) estimated the accretion rate based on the optical disk luminosity, and assumed $\eta = 1$ in Eq. (3) to obtain $\dot{M}_2 \approx 3 \times 10^{-12} M_{\odot} \text{yr}^{-1}$ (EZ Lyn* in Fig. 2). Galiullin et al. (2024) incorporated a bolometric correction to the X-ray luminosity, which assumed a thermal bremsstrahlung model for the emission, to obtain $\dot{M}_2 \approx (1.7 - 7.8) \times 10^{-12} M_{\odot} \text{yr}^{-1}$ (SRGeJ0411+6853* in Fig. 2). However, they did not explore a range of radiative efficiencies. In both cases, the accretion rates could have been underestimated. Another reason why these may be underestimated is because their \dot{M}_2 (lower end of SRGeJ0411+6853*) are smaller than that by our $\kappa = 0$ model. Assuming that the CV remains semidetached, the estimates by the $\kappa = 0$ model set the minimum accretion rate post-bounce. Regardless, the \dot{M}_2 of EZ Lyn* is only a factor of 2 smaller than that predicted by our $\kappa = 15B^4$ model. It will agree with our model if we choose $\eta = 0.5$ in Eq. (3) to calculate \dot{M}_2 . The \dot{M}_2 of SRGeJ0411+6853* is already in general agreement with both the $\kappa = 15B^2$ and $\kappa = 15B^4$ models. Our model tracks agree well with several systems in Fig. 2, but notably our $\kappa = 15B^4$ model is in good agreement with all the estimates of SDSSJ1501 and SDSSJ1035, namely P_{orb} , M_2 and \dot{M}_2 , while our $\kappa = 15B^2$ model is in agreement with the P_{orb} and M_2 estimate of EZ Lyn and within a factor of 2 of its \dot{M}_2 estimate.

3. Physical processes driving the weakening of magnetic braking

We highlight a few physical processes that may cause the weakening of magnetic braking in short-period CVs. We note that this list is not exhaustive and there can be additional mechanisms driving such a weakening.

3.1. Dynamo action in cool stars

In Sect. 2.2 we showed that if the strong-field dynamo proposed by Morin et al. (2011) operates in short-period CV donors, Eq. (1) causes B to reduce significantly for $M_2 \lesssim 0.07M_\odot$. There is observational evidence to suggest that stars with $T_{\text{eff}} \lesssim 2200$ K such as L-dwarfs experience a significant decrease in their chromospheric activity despite being rapid rotators (Mohanty & Basri 2003). This means that the magnetic field strength drops from fully convective M-dwarfs to brown dwarfs. In Sect. 2.2 we show that this drop is due to the change in the mass-radius relation of the star. The results of the α^2 dynamo model proposed by Chabrier & Küker (2006) also show, in accordance with that by Morin et al. (2011), that there is a transition in the magnetic field structure from a steady, large-scale field in late M-dwarfs to a toroidal, oscillatory field in brown dwarfs. In addition, the conductivity of the atmosphere of cool objects such as brown dwarfs decreases greatly, thereby hampering the formation of a hot corona which drives stellar winds. The combined effect of weaker stellar winds and reduced magnetic field strength drives a weaker MB in brown dwarfs (Mohanty & Basri 2003; Chabrier & Küker 2006). In other words, if such a dynamo operates in short-period CV donors, MB reduces significantly as the donor enters the brown dwarf regime ($M_2 \lesssim 0.07M_\odot$).

3.2. White dwarf magnetism

Isern et al. (2017) suggested that cool WDs generate strong magnetic fields by a crystallization-driven dynamo. Schreiber et al. (2021) showed that magnetic CVs can be explained by the rapid rotation and crystallization of the WD accretors, which can generate fields of several MG (Ginzburg et al. 2022). Schreiber et al. (2023) recently proposed that such fields are generated in the accretor of short-period CVs post period minimum. This field connects with that of the donor star, resulting in the detachment of period bouncers for several Gyr. They argue that this can lead to about a 60% reduction in the observed period-bouncer CVs.

We illustrate a variation in their analysis where the CV may remain semidetached. Schreiber et al. (2023) assume that the diffusion timescale of the magnetic field to the WD surface is 100 Myr (Fig. 3 of Ginzburg et al. 2022). However, recently Blatman & Ginzburg (2023) showed that the magnetic field on the WD surface gradually emerges on a Gyr timescale (their bottom right subplot in Fig. 1). By consistently taking into account phase separation, they find that the magnetic diffusion time is about a Gyr at the time of breakout and shortly afterward (this also depends on the WD mass). The donor has its thermal timescale about a few Gyr depending on the mass-transfer rate. Since the thermal timescale of the donor is comparable to the diffusion timescale of the WD magnetic field, there is a possibility that the donor adjusts to the reduction in MB because of magnetic reconnection post-period minimum while continually filling its Roche lobe. In such a case, the evolution will be similar to that given in Sect. 2. However, such a weakening depends on the properties of the WD accretor, such as its mass and temperature, but is independent of the donor star transitioning from

an M-dwarf to a brown dwarf. So, such systems would not necessarily experience a MB weakening at $M_2 \approx 0.07M_\odot$ but when the WD becomes magnetic (Schreiber et al. 2023).

3.3. Dead zones

The dead zone is the region around a spinning magnetized star where the stellar wind is captured and forced to corotate along its magnetic field lines (Mestel & Spruit 1987). This leads to a reduction of wind mass loss and, as a consequence, the strength of MB. Dead zones were first studied by Mestel & Spruit (1987) who gave a simple description for isolated solar-like stars with different rotation rates. Subsequently, several groups have implemented the effects of dead zones in their calculations of MB torque in stellar spin-down (Réville et al. 2015; Garraffo et al. 2015). Because dead zones arise through the interplay of gravity, centrifugal force, and magnetism in the star, they should be at play in every system undergoing MB. This includes the donor stars in CVs. The only difference here is that, owing to tidal locking, P_{orb} governs the behavior of the dead zone. We calculate the evolution of dead zones using the simple treatment of Mestel & Spruit (1987, their Eqs (8) and (9)), adopting solar parameters for the coronal temperature and mean molecular weight. The choice of these parameters does not alter the qualitative behavior of our dead zone calculation.

For the expression of the ratio of the magnetic pressure and the thermal pressure at the base of the dead zone ζ_d , we study the behavior of two cases: $\zeta_d = 60(\Omega/\Omega_\odot)$ and $\zeta_d = 60(\Omega/\Omega_\odot)^2$, in their Table 1. Here Ω is the orbital angular velocity of the CV. The evolution of the dead zone of the donor star for the models with constant κ in Fig. 1 is shown in Fig. 3. Here $f_{\text{DZ}} = R_2/R_{\text{DZ}}$ is the fraction of field lines contributing to MB in the system, where R_{DZ} is the equatorial radius of the dead zone. With no dead zones $f_{\text{DZ}} = 1$. The value $f_{\text{DZ},i}$ denotes the contribution of dead zones at the time of commencement of RLOF⁶. These tracks demonstrate how the dead zones would behave in a short-period CV. We see that when $\zeta_d \propto \Omega$, f_{DZ} changes very little throughout the evolution. However, the dead zones grow (f_{DZ} becomes smaller) with decreasing M_2 when $\zeta_d \propto \Omega^2$, with the drop becoming steep at $M_2 \approx 0.05M_\odot$. A stronger dependence of ζ_d on Ω yields a steeper drop in f_{DZ} . One way in which MB affects dead zones is through the generated magnetic field in the donor (say, by a strong-field dynamo or an α^2 dynamo) which governs the magnetic pressure outside the star (through ζ_d). Dead zones work as an additional mechanism of MB alteration which is always at play regardless of the physical mechanism that drives MB. It can further weaken MB if $d \ln \zeta_d / d \ln \Omega \gtrsim 2$ (Fig. 3).

4. Conclusion

In this Letter, we have shown that the weakening of magnetic braking in short-period CVs can explain the current dearth of observed period bouncers. We find that the weakening of magnetic braking around the period minimum stalls the evolution of CVs around the observed period minimum spike between 80 and 86 min. This makes them difficult to distinguish from pre-bounce systems. When they evolve post-period minimum, their mass-transfer rate decreases below the current detectable threshold. We predict the system properties of fainter period bouncer candidates that upcoming surveys such as SRG/eROSITA can

⁶ We note that this plot is made post-evolution so that dead zones do not alter the MB strength of these models.

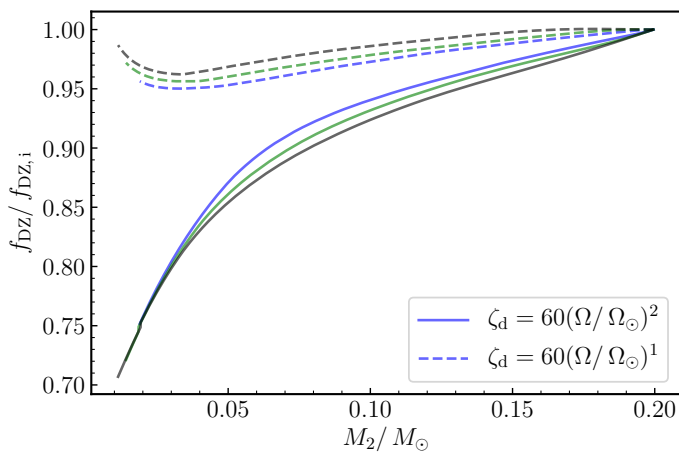


Fig. 3. The evolution of the dead zone relative to that at the beginning of RLOF $f_{DZ}/f_{DZ,i}$ with M_2 for the models with constant κ . The colors denote the same models as in Figs 1 and 2, with $\kappa = 0$ shown in blue, $\kappa = 4$ in green and $\kappa = 15$ in black. The line styles denote the choice of ζ_d . The dead zone for each track is calculated post-evolution by the method of Mestel & Spruit (1987).

likely detect. We discuss how the weakening of magnetic braking can be caused by physical processes such as a change in the dynamo action in the donor, the emergence of magnetism in the white dwarf accretor and dead zones in the donor trapping stellar winds. An accurate estimate of the relative fraction of period bouncers with this formalism will be obtained with a population synthesis study which we shall undertake in the future.

Acknowledgements. AS thanks the Gates Cambridge Trust for his scholarship. AS also thanks Ken Shen and Elmé Breedt for discussions on the nature of short-period cataclysmic variables. ACR acknowledges support from an NSF Graduate Research Fellowship. AS and ACR are grateful to Franco Giovanelli and the Golden Age of Cataclysmic Variables and Related Objects VI Workshop for facilitating fruitful conversations. SG acknowledges support from the Israel Ministry of Innovation, Science, and Technology (grant No. 1001572596), and from the U.S. – Israel Binational Science Foundation (BSF; grant No. 2022175). AS and SG thank Daniel Blatman for the discussion on the emergence of magnetic fields in white dwarfs. CAT thanks Churchill College for his fellowship.

References

- Amantayeva, A., Zharikov, S., Page, K. L., et al. 2021, *ApJ*, 918, 58
 Blatman, D. & Ginzburg, S. 2023, arXiv e-prints, arXiv:2311.09299
 Chabrier, G. & Küker, M. 2006, *A&A*, 446, 1027
 Galiullin, I., Rodríguez, A. C., Kulkarni, S. R., et al. 2024, arXiv e-prints, arXiv:2401.04178
 Gänsicke, B. T., Dillon, M., Southworth, J., et al. 2009, *MNRAS*, 397, 2170
 Garraffo, C., Drake, J. J., & Cohen, O. 2015, *ApJ*, 813, 40
 Ginzburg, S., Fuller, J., Kawka, A., & Caiazzo, I. 2022, *MNRAS*, 514, 4111–4119
 Goliash, J. & Nelson, L. 2015, *ApJ*, 809, 80
 Inight, K., Gänsicke, B. T., Schwöpe, A., et al. 2023, *MNRAS*, 525, 3597
 Isern, J., García-Berro, E., Külebi, B., & Lorén-Aguilar, P. 2017, *ApJ*, 836, L28
 Jermyn, A. S., Bauer, E. B., Schwab, J., et al. 2023, *ApJS*, 265, 15
 Knigge, C. 2006, *MNRAS*, 373, 484
 Knigge, C., Baraffe, I., & Patterson, J. 2011, *ApJS*, 194, 28
 Kolb, U. 1993, *A&A*, 271, 149
 Kollmeier, J. A., Zasowski, G., Rix, H.-W., et al. 2017, arXiv e-prints, arXiv:1711.03234
 Li, J. K., Wu, K. W., & Wickramasinghe, D. T. 1994, *MNRAS*, 268, 61
 Littlefair, S. P., Dhillon, V. S., Marsh, T. R., et al. 2008, *MNRAS*, 388, 1582
 Liu, F. K., Meyer, F., Meyer-Hofmeister, E., & Burwitz, V. 2008, *A&A*, 483, 231
 McAllister, M. J., Littlefair, S. P., Dhillon, V. S., et al. 2017, *MNRAS*, 467, 1024
 Mestel, L. & Spruit, H. C. 1987, *MNRAS*, 226, 57
 Mohanty, S. & Basri, G. 2003, *ApJ*, 583, 451
 Morin, J., Donati, J. F., Petit, P., et al. 2010, *MNRAS*, 407, 2269
 Morin, J., Dormy, E., Schrunner, M., & Donati, J. F. 2011, *MNRAS*, 418, L133

- Muñoz-Giraldo, D., Stelzer, B., de Martino, D., & Schwöpe, A. 2023, *A&A*, 676, A7
 Mukai, K. 2017, *PASP*, 129, 062001
 Narayan, R., McClintock, J. E., & Yi, I. 1996, *ApJ*, 457, 821
 Narayan, R. & Popham, R. 1993, *Nature*, 362, 820
 Neustroev, V. V. & Mäntynen, I. 2023, *MNRAS*, 523, 6114
 Paczynski, B. & Sienkiewicz, R. 1981, *ApJ*, 248, L27
 Pala, A. F., Gänsicke, B. T., Belloni, D., et al. 2022, *MNRAS*, 510, 6110
 Pala, A. F., Gänsicke, B. T., Breedt, E., et al. 2020, *MNRAS*, 494, 3799
 Pala, A. F., Schmidtobreick, L., Tappert, C., Gänsicke, B. T., & Mehner, A. 2018, *MNRAS*, 481, 2523
 Paxton, B., Bildsten, L., Dotter, A., et al. 2011, *ApJS*, 192, 3
 Paxton, B., Cantiello, M., Arras, P., et al. 2013, *ApJS*, 208, 4
 Paxton, B., Marchant, P., Schwab, J., et al. 2015, *ApJS*, 220, 15
 Paxton, B., Schwab, J., Bauer, E. B., et al. 2018, *ApJS*, 234, 34
 Paxton, B., Smolec, R., Schwab, J., et al. 2019, *ApJS*, 243, 10
 Predehl, P., Andritschke, R., Arefiev, V., et al. 2021, *A&A*, 647, A1
 Réville, V., Brun, A. S., Matt, S. P., Strugarek, A., & Pinto, R. F. 2015, *ApJ*, 798, 116
 Rodríguez, A. C. 2024, arXiv e-prints, arXiv:2401.09537
 Sarkar, A. & Tout, C. A. 2022, *MNRAS*, 513, 4169
 Sarkar, A., Yungelson, L., & Tout, C. A. 2023, *MNRAS*, 526, 870
 Schreiber, M. R., Belloni, D., Gänsicke, B. T., Parsons, S. G., & Zorotovic, M. 2021, *Nature Astronomy*, 5, 648
 Schreiber, M. R., Belloni, D., & van Roestel, J. 2023, *A&A*, 679, L8
 Sunyaev, R., Arefiev, V., Babyshkin, V., et al. 2021, *A&A*, 656, A132
 Townsley, D. M. & Bildsten, L. 2004, *ApJ*, 600, 390
 Warner, B. 2003, *Cataclysmic Variable Stars* (Cambridge University Press)

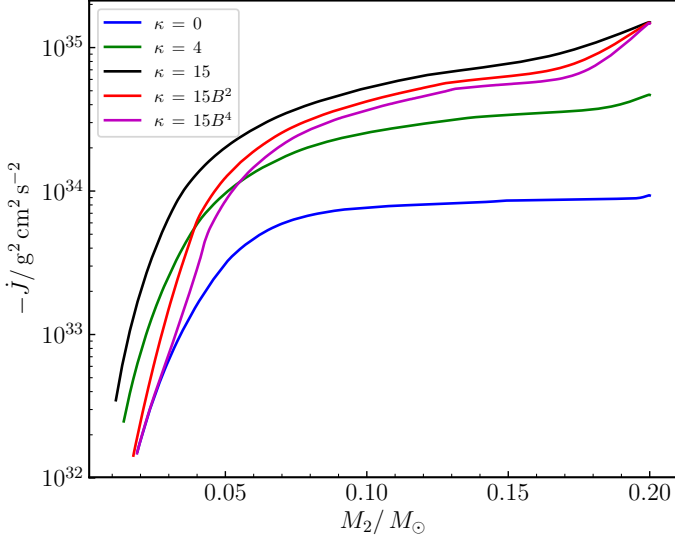


Fig. B.1. The evolution of \dot{J} with M_2 for the models in Fig. 1.

Appendix A: A catalog of period bouncers

We present a catalog of all known period bouncers in Table A.1. While there are more (some 25 to 30 in total) such candidate systems in the literature, we require there to be precise estimates of 1) an orbital period, 2) donor mass, 3) WD mass (and radius) and 4) WD temperature for us to include it in our sample. If a donor mass is not available, we ensure that WD properties are well-measured and that there is spectroscopic evidence for a brown dwarf donor. We also indicate the few systems known to be eclipsing, because those have, on the whole, more precisely measured donor star parameters.

Appendix B: Evolution of angular momentum loss

In Fig. B.1 we plot the evolution of the total angular momentum loss $\dot{J} \equiv \text{AML}_{\text{GWR}} + \text{AML}_{\text{MB}}$ with the donor mass. Note that although $-\dot{J}$ decreases throughout the evolution for each model, at $M_2 \approx 0.07 M_\odot$ it decreases more steeply for the models where κ depends on stellar parameters.

Name	$P_{\text{orb}}/ \text{hr}$	Ecl.?	M_2/ M_{\odot}	M_{WD}/ M_{\odot}	$R_{\text{WD}}/ 0.01 R_{\odot}$	$T_{\text{eff, WD}}/ \text{K}$	$\dot{M}_2/ 10^{-10} M_{\odot} \text{yr}^{-1}$	Ref.
EZ Lyn	1.430	Yes	0.042±0.014	0.85±0.01	0.94	11250±40	0.242 ^{+0.003} _{-0.003}	1
SDSSJ1035 + 0551	1.370	Yes	0.052±0.002	0.94±0.01	0.87±0.01	10100±200	0.12 ^{+0.005} _{-0.005}	2
SDSSJ1057 + 2759	1.510	Yes	0.0436±0.002	0.80±0.015	1.04±0.017	13300±1100	0.54 ^{+0.14} _{-0.17}	3
SDSSJ1433 + 1011	1.300	Yes	0.06±0.003	0.868±0.007	0.958±0.008	12800±200	0.38 ^{+0.02} _{-0.02}	2
SDSS J1501+5501	1.364	Yes	0.053±0.003	0.80±0.03	1.04±0.04	12500±200	0.426 ^{+0.009} _{-0.01}	2
SRGeJ0411+6853	1.625	Yes		0.84±0.07	1.0±0.09	13790±500	0.56 ^{+0.04} _{-0.04}	4
EG Cnc	1.439	No		1.03±0.05	0.77 ^{+0.06} _{-0.05}	12290±55	0.2 ^{+0.03} _{-0.03}	5
GD 552	1.712	No		0.78±0.04	1.07 ^{+0.05} _{-0.04}	10760±40	0.25 ^{+0.02} _{-0.03}	5
1RXS J1050–1404	1.476	No		0.77±0.03	1.08 ^{+0.04} _{-0.03}	11520±50	0.34 ^{+0.02} _{-0.03}	5
QZ Lib	1.539	No		0.82±0.19	1.01 ^{+0.23} _{-0.18}	11420±200	0.28 ^{+0.1} _{-0.2}	5
SDSS J1435+2336	1.300	No		0.84±0.07	1.0 ^{+0.08} _{-0.09}	12000±160	0.32 ^{+0.05} _{-0.05}	5
BW Scl	1.304	No	0.051±0.006	1.007±0.01	0.8 ^{+0.014} _{-0.011}	15145±50	0.51 ^{+0.01} _{-0.008}	5, 6
GW Lib	1.279	No		0.83±0.12	1.03 ^{+0.15} _{-0.10}	16166±350	1.09 ^{+0.26} _{-0.34}	5
WZ Sge	1.360	No		0.80±0.02	1.05 ^{+0.03} _{-0.03}	13190±115	0.53 ^{+0.01} _{-0.01}	5

Table A.1. Known period bouncers with either a well-measured donor mass or accretion rate (derived from WD mass and temperature estimates, Eq. 2). Ecl. stands for eclipsing. *References:* (1) Amantayeva et al. (2021); (2) Littlefair et al. (2008); (3) McAllister et al. (2017); (4) Galiullin et al. (2024); (5) Pala et al. (2022); (6) Neustroev & Mäntynen (2023).